DOI: 10.1002/adma.200602136

Yielding of Metallic Glass Foam by Percolation of an Elastic Buckling Instability**

By *Marios D. Demetriou,* Jay C. Hanan, Chris Veazey, Marco Di Michiel, Nicolas Lenoir, Ersan Üstündag,* and William L. Johnson*

Recent advances in the processing of closed-[1–5] and open-cell[6–9] metallic glass foam have focused increasing attention on the mechanical behavior of this emerging structural material. This interest evolved after recognizing that metallic glasses impregnated with pores can be effectively alleviated from their inherent brittle nature and yet retain a considerable fraction of their outstanding strength.[10] The mechanical behavior of open- and closed-cell metallic glass foams has recently been assessed by means of compressive experiments performed using standard mechanical testing procedures. Open-cell $Zr_{57}Nb_5Cu_{15.4}Ni_{12.6}Al_{10}$ foams investigated in the porosity range of 72–86 % are found to exhibit impressive compressive plasticity extending to nearly 80 % strains, however, they are found to yield at relatively low stresses ranging between 5 and 34 MPa.[7–9] In contrast, closed-cell $Pd_{43.5}Ni_{7.5}Cu_{30}P_{20}$ and $Pd_{35}Pt_{15}Cu_{30}P_{20}$ foams investigated in the porosity range of 36–64 % were found to exhibit substantially higher strengths, ranging between 250 and 600 MPa, but a more modest plasticity ranging between 20 and 30 % strains.[4,5] Plasticity in these closed-cell foams is shown to propagate by recurring non-catastrophic crushing events associated with the formation of collapse bands through the foam structure. More interestingly, ahead of a crushing event these foams are found to exhibit an unusual yielding response characterized by an extended stress plateau. This nonlinear foam yielding response bears resemblance to the yielding of a monolithic metallic glass near zero temperature.[11–13] This resemblance hints at a possible similarity between floppy-bonded networks (such as foams) and zero-temperature glasses, as originally proposed by Alexander.[14] In this communication we seek to investigate the underlying mechanisms governing the nonlinear yielding of these closed-cell foams by examining the intercellular interactions within a bulk-foam specimen by using real-time X-ray microtomography.

For the loading experiment, we utilized a 70 % porosity closed-cell amorphous $Pd_{43}Ni_{10}Cu_{27}P_{20}$ foam. In situ X-ray microtomography during loading was performed at beam line ID15A of the ESRF.[15,16] A cycle involving compressive loading towards a non-catastrophic collapse event followed by unloading was implemented. 18 radiographic images of the cellular structure were recorded at constant strain. The stress–strain diagram is presented in Figure 1. The stress spikes appearing in the loading curve are a consequence of ra-

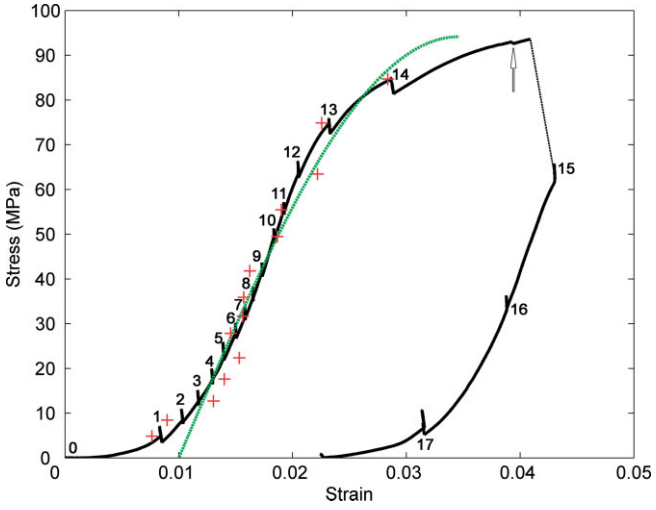

Figure 1. Stress–strain diagram associated with compressive loading of the foam towards a non-catastrophic collapse event and subsequent unloading (black line). The labels indicate the loading states at which tomographic data was recorded. The arrow indicates the onset of local plastic (shear-band) events. An approximation using the cooperative yielding model, Equation 1, using $E = 6.0$ GPa and $\gamma_c = 0.035$ is shown by the green dots. The strain calculated by tracking cell displacements is shown by the red crosses.

[*] Dr. M. D. Demetriou, Dr. C. Veazey, Prof. W. L. Johnson
Keck Laboratory, California Institute of Technology
Pasadena, CA 91125 (USA)
E-mail: marios@caltech.edu
Prof. E. Üstündag
Materials Science and Engineering, Iowa State University
Ames, IA 50011 (USA)
E-mail: ustundag@iastate.edu
Prof. J. C. Hanan
Mechanical and Aerospace Engineering, Oklahoma State University
Tulsa, OK 74106 (USA)
Dr. M. Di Michiel
European Synchrotron Radiation Facility
BP220, 38043 Grenoble (France)
Dr. N. Lenoir
Laboratoire 3S
BP 53, 38041 Grenoble (France)

[**] The authors would like to acknowledge valuable discussions with K. Samwer, J. Schroers, R. D. Conner, S. Bossuyt, R. Birringer, M.-A. Nicolet, and L. A. Dunning, and the contributions of A. R. Kinnamon in the image analysis and of M. Kretzschmer in the construction of the loading fixture at the ESRF. Supporting Information is available online from Wiley InterScience or from the authors.

ADVANCED MATERIALS

diography: radiation exposure gave rise to a spontaneous temperature rise, which was effectively accommodated by a stress rise due to the inability of the constrained sample to thermally expand. At low to moderate stress levels these stress spikes undergo complete recovery, whereas at higher stress levels a small residual effect is observed. Nonetheless, the overall damage to the cellular structure caused by radiography was determined from the rendered tomographs to be small compared to the damage caused by deformation.

The stress–strain diagram of Figure 1 reveals that the loading response of the foam initiates in a brief highly compliant regime, which is followed by a linear regime associated with a modulus of ca. 6 GPa. The loading response subsequently undergoes a gradual transition to nonlinearity, and ultimately terminates in a non-catastrophic collapse at 94 MPa. Upon unloading, the foam undergoes a linear response characterized by a modulus that appears essentially unaffected by the collapse. At the conclusion of the cycle, an irreversible strain of 2.3 % is recorded. Despite such large irreversible strain, the unloaded foam specimen appears intact and no macroscopic damage can be detected (see the Supporting Information).

Images obtained from the 3D rendering of the tomography are presented in Figure 2. A 3D-rendered view of the upper half of the foam-specimen gauge section showing the global position of the plane considered for analysis is presented in Figure 2a. The analysis plane is presented in its initial unloaded state (state 0) in Figure 2b. In Figure 2c, images of that segment at loading states 1–11 are superimposed in an effort to demonstrate the evolution of linear deformation. The uniform blurring depicted in this composite image qualitatively demonstrates that deformation in the linear regime is homogeneous. Deformation during the nonlinear response, demonstrated in Figure 2d by superimposing images from states 12–14, appears to be rather localized along an intermediate transverse plane. The collapse, depicted in Figure 2e by superimposing images from states 14 and 15, appears to be highly inhomogeneous and is shown to evolve along the regions of localized yielding.

By tracking the displacements of cells in the rendered images, displacement fields at discrete loading states were generated. The displacement fields at states 11, 13, 14, and 15 are presented in Figure 3. Strains were calculated as gradients of the displacement fields. The calculated strains, which are superimposed in the stress–strain diagram of Figure 1, verify the nonlinear yielding tendency of these foams. By inspecting the displacement fields in Figure 3, it can be observed that the nonaffine cell displacements (i.e. the deviations from the average displacement), which appear relatively small up to state 14, dramatically diverge at state 15 producing a large offset of 0.375 mm. The permanent deformation in the specimen after unloading is measured to be 0.40 mm. It is therefore suggested that the majority of irreversibilities realized during the loading cycle occurred between states 14 and 15. Plasticity in metallic glasses is known to be accommodated by shear banding, which is manifested in the stress–strain response as serrated flow.[17] Serrations designating local plastic

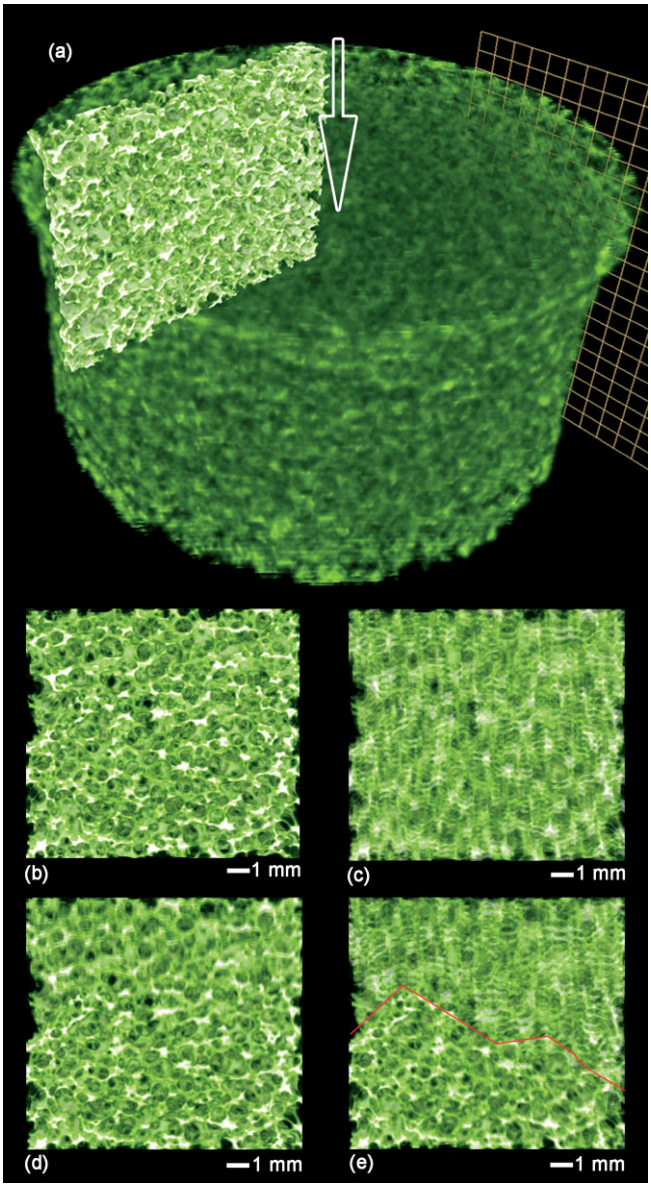

Figure 2. 3D-rendered view of the cellular structure during loading. a) Upper half of the foam-specimen gauge section showing the global position of the analysis plane. The arrow indicates the direction of loading; b) Analysis plane in the unloaded state (state 0); c) Deformation in the linear regime (states 1–11 overlapped); d) Deformation in the nonlinear regime (states 12–14 overlapped); e) Deformation upon non-catastrophic collapse (states 14–15 overlapped). The line marks the regions of collapse.

events within the glassy solid can be detected ahead of the collapse event (see the arrow in Figure 1 and Wada et al.[4,5]). However the energy dissipated during those plastic events (which scales with the stress serration amplitude) appears small compared to the energy dissipated upon collapse, suggesting that a considerable fraction of the energy release during collapse is essentially stored elastic energy.

Nonlinear elasticity in foams is known to be accommodated by strut buckling.[18] The stability of struts against Eulerian

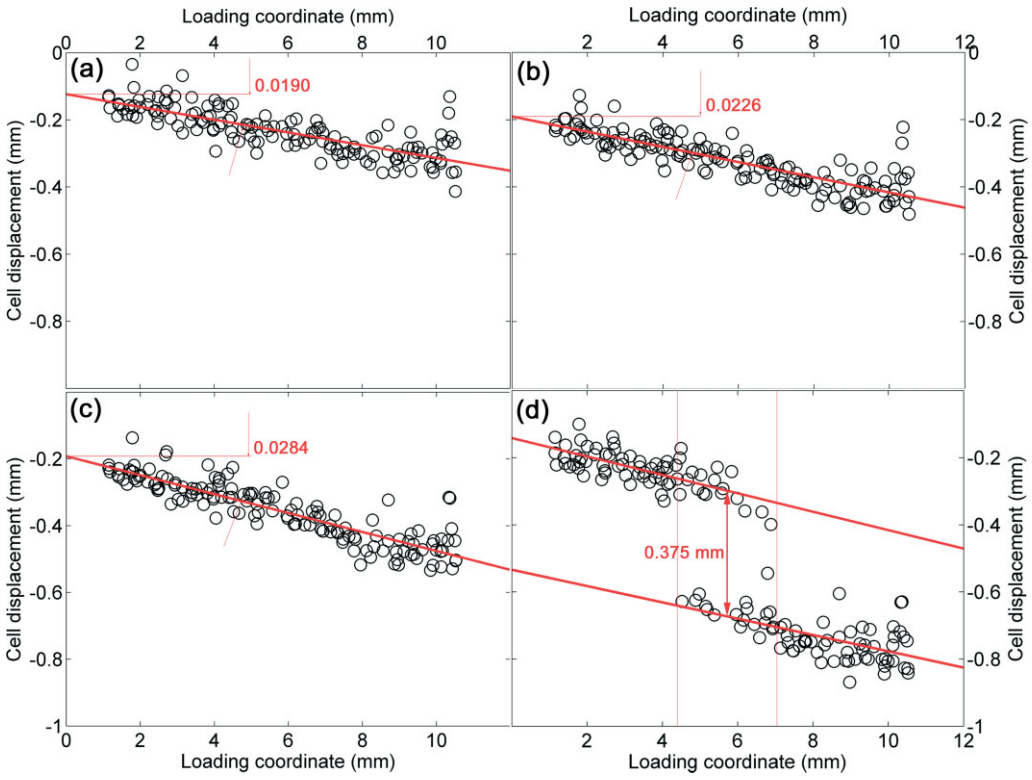

Figure 3. Cell displacements versus cell coordinates along the loading direction, evaluated by tracking cells in the 2D-rendered images: a) state 11; b) state 13; c) state 14; d) state 15. The lines are linear regressions to the data. The slopes of the linear regressions in (a–c) are indicated, which represent global strains associated with the loading states. The vertical lines in (d) indicate the breadth of collapse propagation, whereas the arrow indicates the size of the offset.

buckling is determined by a critical aspect ratio, which for an ideal column is given by $\sqrt{(\pi^2 E/\sigma_y)}$,[19] where σ_y/E is the elastic strain limit of the solid. Owing to their high elastic limit, metallic glasses are expected to become unstable against buckling at relatively low aspect ratios. Specifically, $Pd_{43}Ni_{10}Cu_{27}P_{20}$ is known to have an elastic strain limit of 0.017,[4] which implies that struts having aspect ratios greater than 24 would be unstable against buckling. By means of optical microscopy, membranes having aspect ratios ranging from 5 to 50 have been detected at random regions in the cellular structure of these foams.[20,21] These cellular structures therefore exhibit a rather broad distribution of flexural rigidities and can thus be considered stochastic.

In Figure 4a we present a magnified 3D-rendered view of the yielding region at states 0 (initial), 12, 14, and 15. Closer inspection within the yielding region reveals that the length scale characterizing nonaffine displacement is approximately 0.5 to 1.0 mm, that is, on the order of 4–6 cells. The initial density of the region that ultimately yielded was computed from the rendered data (tomograph 0) to be 25–30 % lower than the bulk foam density,[22] which suggests that cell clusters within this region initially incorporated high-aspect-ratio membranes. The field of view of the camera chosen to record cell displacements in this bulk foam specimen was fairly wide, and therefore the resultant tomographic voxel size is rather large (14 μm pixel^{-1}) and cannot provide adequate information for the structural intracellular transitions. Tomographic data from a smaller (and lees porous) foam specimen gathered using a narrower field of view (1.4 μm pixel^{-1} voxel size) was substantially more resolved within intracellular regions and therefore more revealing of the intracellular transitions. 2D-rendered images from that data are presented in Figure 4b. These images reveal that the structural intracellular transitions evolve by membrane-buckling events, which within the yielding region approach the limit of instability causing membrane rupture.

The tomographic data therefore suggests that the apparent nonlinear yielding of these foams is associated with the development of an elastic stress field within the structure to accommodate a sequence of membrane-buckling instabilities. The fundamental defects in this process are thus identified to be "soft" cell clusters incorporating slender membranes prone to buckling. Given the stochastic geometry of the cellular structure, it is reasonable to assume that the evolution of global collapse is a result of the percolation of these randomly distributed buckling instabilities. When buckling instabilities ultimately percolate, the total elastic energy stored in the accommodating stress field is dissipated by a mechanism of localized shearing, giving rise to the formation of the collapse band. In catastrophe theory, Eulerian buckling is mathematically treated as a cusp

ADVANCED MATERIALS

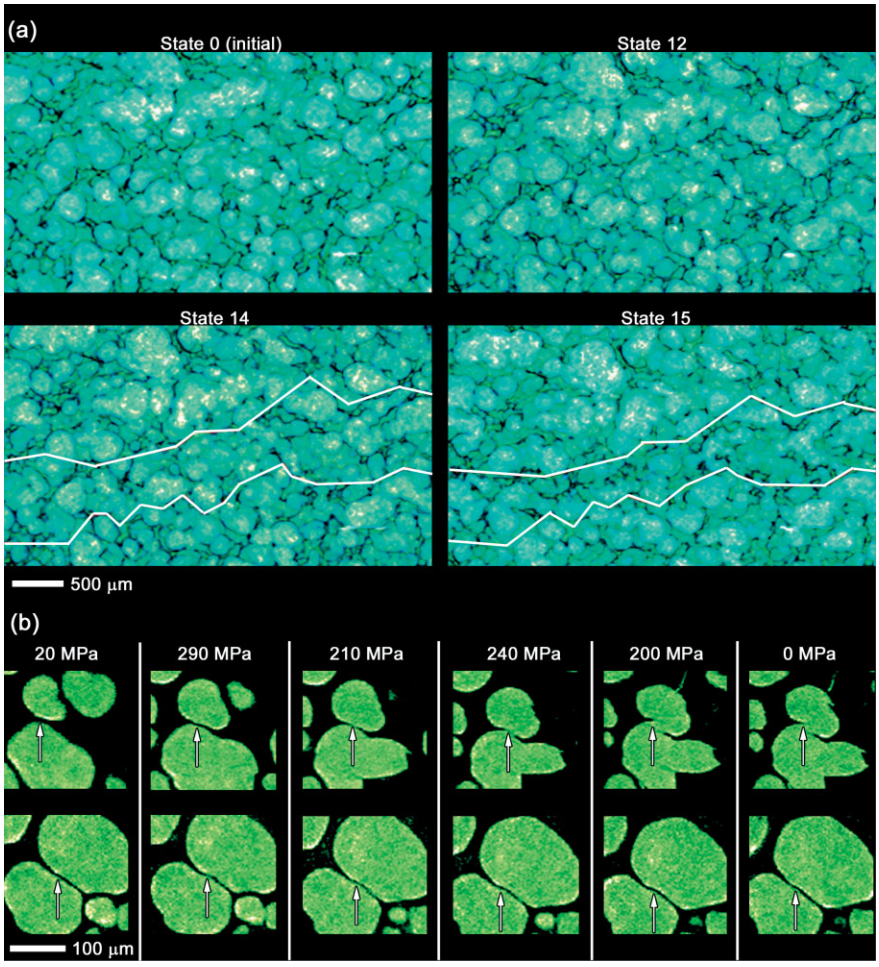

Figure 4. a) Magnified 3D-rendered view of the yielding region at states 0, 12, 14, and 15. The lines in the images of state 14 and 15 indicate the yielding region, which appears approximately 4–6 cells wide. Yielding in this region is shown to be accommodated by cooperative shearing of neighboring cell clusters. b) 2D-rendered images from the tomographic data gathered using a 1.4 μm pixel^{-1} voxel size. A smaller (and less porous) foam specimen was utilized in this tomography experiment. The stress level at each tomographic state is indicated. In the upper row, the interaction between two neighboring cells within the yielding region is demonstrated. (Note that due to the fixed planar view depicted in these 2D images, some out-of-plane motion owing to lateral deformation can be visualized.) The intracellular deformation is shown to evolve by a buckling mechanism, which ultimately becomes unstable leading to membrane rupture. In the lower row, the interaction between two neighboring cells outside the yielding region is demonstrated. The intracellular deformation also appears to evolve by buckling, which however remains stable and is followed by reversible unbuckling upon unloading.

catastrophe, that is, a second-order phase transition.[23] The possible buckling modes of membranes within a cell cluster can therefore be thought of as instabilities of configurational inherent states. Taking ϕ_0 to be the average barrier-energy density for configurational hopping to a buckled state, γ to be the overall global configurational strain, and γ_c the average strain per cluster at shear instability, the periodic elastic energy density ϕ can be expressed as $\phi/\phi_0 = \sin^2(\pi\gamma/4\gamma_c)$. This treatment is analogous to that employed by Frenkel to analyze cooperative yielding of a dislocation-free crystal,[24] and was recently adopted by Johnson and Samwer to model cooperative yielding of a shear transformation zone in a metallic glass.[25] This formulation can be extended to a nonlinear shear stress–strain relation as $\tau = \delta\phi/\delta\gamma = (\pi\phi_0/4\gamma_c)\sin(\pi\gamma/2\gamma_c)$. Relating ϕ_0 to an average shear modulus $G = d^2\phi/d\gamma^2\,|_{\gamma=0} = \pi^2\phi_o/8\gamma_c^2$, the τ–γ relation becomes $\tau = (2/\pi)G\gamma_c\sin(\pi\gamma/2\gamma_c)$. Defining E and ν as the average Young's modulus and Poisson's ratio, we can approximate this τ–γ relation by a uniaxial σ–ε relation (assuming the structure is on average isotropic), as follows

$$\sigma = \frac{2}{\pi}\frac{E}{(1+\nu)}\gamma_c \sin\left(\frac{\pi}{2}\frac{\varepsilon}{\gamma_c}(1+\nu)\right) \qquad (1)$$

By substituting $E = 6$ GPa and $\nu = 0.42$[26] for the present foam, Equation 1 is shown to capture the overall yielding response reasonably well for $\gamma_c \sim 0.035$ (Fig. 1). Furthermore, in Figure 5 we show that Equation 1 is capable of capturing the yielding responses of other closed-cell $Pd_{42.5}Ni_{7.5}Cu_{30}P_{20}$[4] foams with different porosities. These foams are found to exhibit γ_c values of 0.036, 0.033, and 0.035 ($\nu = 0.42$ for all foams[26]). A scaling tendency between the collapse stress of these foams, σ_c, and the amplitude of Equation 1, $E\gamma_c/((\pi/2)(1+\nu))$, is therefore implied. Using the data reported for the collapse stress and modulus of all the similar foams tested to date, which involve seven $Pd_{42.5}Ni_{7.5}Cu_{30}P_{20}$,[4] one $Pd_{35}Pt_{15}Cu_{30}P_{20}$,[5] and the present $Pd_{43}Ni_{10}Cu_{27}P_{20}$, a fairly tight correlation between σ_c and $E\gamma_c/((\pi/2)(1+\nu))$ can be constructed (Fig. 6). The correlation is 99 % accurate, and reveals a value for γ_c of 0.03598.

We have thus demonstrated that the collapse stress of these foams (in the range of 100 to 600 MPa) accurately scales with the elastic modulus (in the range of 6 to 32 GPa), in accordance with Equation 1. This scaling tendency between failure stress and elastic modulus validates the argument that the dominant foam yielding mechanism is elastic strut buckling, as such scaling has been shown to arise directly from beam theory.[18] More importantly, this scaling tendency reveals a universal shear-stability limit of 0.036, which can be associated with a critical stored elastic-energy density required to accommodate a sequence of percolating buckling instabilities. Equivalently, γ_c can be thought of as the threshold for the rigidity percolation transition by which random local buckling instabilities evolve globally causing the structure to lose its elastic rigidity.

Another system that we can immediately identify that also obeys this limit is the metallic glass at the state of zero tem-

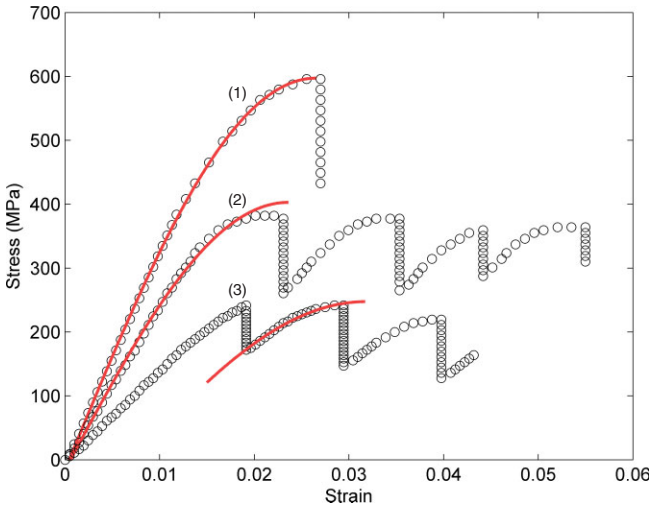

Figure 5. Fit of the cooperative-yielding model, Equation 1, to the mechanical test data reported for $Pd_{42.5}Ni_{7.5}Cu_{30}P_{20}$ foams [4]: experiment (circles); model (red line). 1) 36% porosity: $E = 36.0$ GPa, $\gamma_c = 0.036$; 2) 42% porosity: $E = 27.5$ GPa, $\gamma_c = 0.033$; 3) 64%porosity: $E = 15.6$ GPa, $\gamma_c = 0.035$ (the secondary yielding response is modeled, as the primary response appears interrupted possibly by premature fracture).

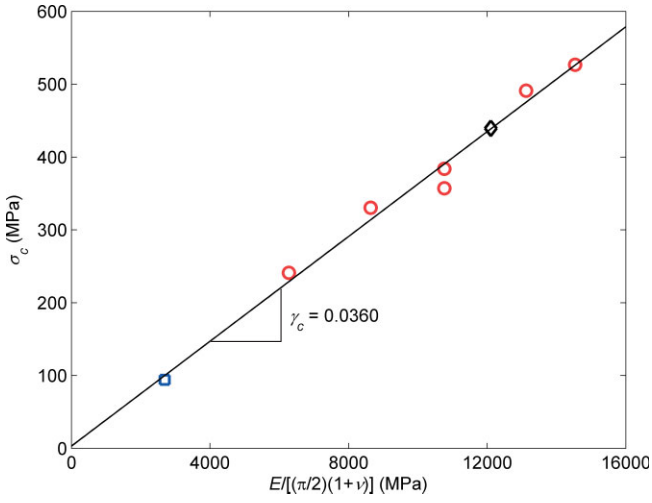

Figure 6. Correlation between σ_c and $E\gamma_c/((\pi/2)(1+\nu))$ using collapse stress and modulus data reported for seven $Pd_{42.5}Ni_{7.5}Cu_{30}P_{20}$ foams (red circles) [4], one $Pd_{35}Pt_{15}Cu_{30}P_{20}$ foam (black diamond) [5], and the present $Pd_{43}Ni_{10}Cu_{27}P_{20}$ foam (blue square). The linear fit is 99% accurate ($R^2 = 0.987$), and exhibits a slope of 0.03598.

perature. At that state, where thermal fluctuations vanish and geometric randomness dominates, the shear elastic limit of metallic glasses is known to be 0.0360 ± 0.0020.[25] This similarity in shear stability essentially implies that the barrier crossing events in the shear transformation zones of a glass can be suitably described by a sequence of Eulerian buckling instabilities. This observation lends experimental support to the early phenomenological theories developed by Alexander,[14] in which zero-temperature glasses are treated as floppy bonded networks prone to Eulerian buckling when stressed. His theories were subsequently validated by molecular dynamics simulations of zero-temperature Lennard–Jones glasses,[27–29] in which nonaffine distortions were correlated to percolating atomic chains effectively acting as the structural buckling membranes of the system. Metallic glass foam conforms well to the mechanisms underlying this class of rigidity percolation transition, and can thus be thought of as a macroscopic configurational model of the zero-temperature metallic glass.

In conclusion, by using real-time X-ray microtomography we detected the nonlinear yielding of metallic glass foam to evolve by percolation of local elastic membrane-buckling instabilities. By means of a nonlinear elasticity analysis, we determined the shear stability of metallic glass foams of various porosities and different base materials to be characterized by a universal strain limit of 0.036. We associate this shear-stability limit with a critical elastic-energy-density storage required to accommodate a sequence of percolating buckling instabilities, and thus identify it as the threshold for the elastic rigidity percolation transition. By recognizing that metallic glasses in their zero-temperature state obey the same universal shear-stability criterion, we reveal a link between floppy modes in a glass and buckling instabilities in a stochastic cellular structure.

Experimental

The 70% porosity closed-cell amorphous $Pd_{43}Ni_{10}Cu_{27}P_{20}$ foam was prepared by expanding an amorphous precursor, as described elsewhere [20,21]. The foam was machined to a tapered test specimen 17.70 mm in height, having a gage section of 8.08 mm in diameter and 8.14 mm in length. The ID15A beam line of ESRF was utilized for the in situ X-ray microtomography experiment [15]. A cylindrical loading fixture specifically built for microtomography experiments with a maximum loading capacity of 7.5 kN was utilized [16]. A strain rate of 2×10^{-5} s^{-1} was applied. Strains were estimated from the crosshead displacement, and were subsequently corrected for the nonlinear machine compliance. The tomographic data recorded at discrete loading states were reconstructed by means of image analysis. A filtered back-projection algorithm [30] was utilized to obtain a 3D representation of the attenuation coefficient of the foam. Amira 3D image-analysis software was employed to separate cells from the solid matrix using 3D volume rendering at a fixed intensity threshold. A $50\times835\times300$ voxel segment in the upper half of the $835\times835\times573$ voxel gauge section was analyzed at the full resolution of 14 μm $pixel^{-1}$. Cell positions in 2D-rendered images were tracked by means of template recognition using IMAQ Vision Builder image-analysis software.

Received: September 19, 2006
Revised: February 17, 2007
Published online: July 12, 2007

[1] J. Schroers, C. Veazey, W. L. Johnson, *Appl. Phys. Lett.* **2003**, *82*, 370.
[2] J. Schroers, C. Veazey, M. D. Demetriou, W. L. Johnson, *J. Appl. Phys.* **2004**, *96*, 7723.
[3] A. H. Brothers, D. C. Dunand, *Appl. Phys. Lett.* **2004**, *84*, 1108.
[4] T. Wada, A. Inoue, *Mater. Trans.* **2004**, *45*, 2761.
[5] T. Wada, K. Takenaka, N. Nishiyama, A. Inoue, *Mater. Trans.* **2005**, *46*, 2777.
[6] T. Wada, A. Inoue, *Mater. Trans.* **2003**, *44*, 2228.

ADVANCED MATERIALS

[7] A. H. Brothers, D. C. Dunand, *Adv. Mater.* **2005**, *17*, 484.
[8] A. H. Brothers, D. C. Dunand, *Acta Mater.* **2005**, *53*, 4427.
[9] A. H. Brothers, D. C. Dunand, *Scripta Mater.* **2006**, *54*, 513.
[10] T. Wada, A. Inoue, A. L. Greer, *Appl. Phys. Lett.* **2004**, *86*, 251 907.
[11] S. Takeuchi, T. Kakegawa, T. Hashimoto, A. -P. Tsai, A. Inoue, Mater. Trans. , *JIM* **2000**, *41*, 1443.
[12] H. Li, C. Fan, K. Tao, H. Choo, P. K. Liaw, *Adv. Mater.* **2006**, *18*, 752.
[13] H. Li, K. Tao, C. Fan, P. K. Liaw, H. Choo, *Appl. Phys. Lett.* **2006**, *89*, 041 921.
[14] S. Alexander, *Phys. Rep.* **1998**, *296*, 65.
[15] M. Di Michiel, J. M. Merino, D. Fernandez-Carreiras, T. Buslaps, V. Honkimäki, P. Falus, T. Martins, O. Svensson, *Rev. Sci. Instrum.* **2005**, *76*, 043 702.
[16] G. Viggiani, N. Lenoir, P. Bésuelle, M. Di Michiel, S. Marello, J. Desrues, M. Kretzschmer, *C. R. Mecanique* **2004**, *332*, 819.
[17] H. S. Chen, *Scripta Metall.* **1973**, *7*, 931.
[18] L. J. Gibson, M. F. Ashby, *Cellular Solids: Structure and Properties.* 2nd Ed. Cambridge University Press, Cambridge **1997**, Ch. 5.
[19] J. M. Gere S. P. Timoshenko, *Mechanics of Materials.* 3rd Ed. PWS-Kent, Boston **1975**, Ch. 9.
[20] M. D. Demetriou, C. Veazey, J. Schroers, J. C. Hanan, W. L. Johnson, *Mater. Sci. Eng. A* **2007**, *449*, 863.
[21] M. D. Demetriou, C. Veazey, J. Schroers, J. C. Hanan, W. L. Johnson, *J. Alloys Comp.* **2007**, *434*, 92.
[22] J. Ma, *Ph.D. Thesis*, Oklahoma State University, Stillwater, OK **2006**, p. 81.
[23] R. Gilmore, *Catastrophe Theory for Scientists and Engineers.* John Wiley & Sons, New York **1981**, p. 258.
[24] J. Frenkel, *Z. Phys.* **1926**, *37*, 572.
[25] W. L. Johnson, K. Samwer, *Phys. Rev. Lett.* **2005**, *95*, 195 501.
[26] The Poisson's ratio of monolithic $Pd_{40}Ni_{10}Cu_{30}P_{20}$ is evaluated acoustically to be 0.395 (see N. Nishiyama, A. Inoue, J. Z. Jiang, *Appl. Phys. Lett.* **2001**, *78*, 1985). To account for the effect of the pores, we assume a slightly higher value ($\nu = 0.42$ for all foams), in accordance with recently reported correlations (see K. K. Phani, D. Sanyal, *J. Mater. Sci.* **2005**, *40*, 5685). It is noted that Equation 1 is rather insensitive to ν, and thus the assumed value for ν has a minimal effect on the model predictions.
[27] T. Kustanovich, S. Alexander, Z. Olami, *Physica A* **1999**, *266*, 434.
[28] T. Kustanovich, Z. Olami, *Phys. Rev. B: Condens. Matter Mater. Phys.* **2000**, *61*, 4813.
[29] T. Kustanovich, Y. Rabin, Z. Olami, *Phys. Rev. B: Condens. Matter Mater. Phys.* **2003**, *67*, 104 206.
[30] see A. C. Kak, M. Slaney, *Principles of Computerized Tomographic Imaging* IEEE, New York **1988**, p. 186.

